

QCD String Structure in Vector Confinement

Theodore J. Allen

*Physics Department, Hobart & William Smith Colleges
Geneva, New York 14456 USA*

Todd Coleman and M. G. Olsson

*Department of Physics, University of Wisconsin,
1150 University Avenue, Madison, Wisconsin 53706 USA*

Siniša Veseli

*Fermi National Accelerator Laboratory
P.O. Box 500, Batavia, Illinois 60510 USA*

(Dated: December 5, 2018)

We demonstrate that the Nambu-Goto string spectroscopy with massless quarks is replicated in highly excited states of the linear vector confinement potential. For deep radial excitations we observe that the Regge slope, spacing between daughter trajectories, and absolute state energies agree with those of the QCD string.

I. INTRODUCTION

We present here an interesting simple observation on electric potential confinement. Our conclusions concern the nature of potential models and their relationship to QCD string confinement. In the case of the time component vector (TCV) potential we note a remarkable transition in the Regge spectroscopy from the leading trajectories with slopes $1/4a$ to deep daughter slopes of $1/\pi a$. In fact, the exact string spectroscopy is found to be embedded in this regime. The latter slope is characteristic of the Nambu-Goto QCD string with one fixed end [1]. We first discuss some general properties of the spinless Salpeter (SS) or square root equation. For the linear TCV potential we then compute the Regge structure in the orbitally and radially dominant regimes.

II. SPINLESS SALPETER EQUATION

The spinless Salpeter equation has long been attractive as a minimal generalization of the non-relativistic Schrödinger equations with relativistic kinematics. Its main difficulty is that it involves the square root of a differential operator, sometimes called a pseudo-differential operator, which is difficult to treat analytically. Even so, it is easily implemented numerically. The introduction of a variational method [2] allowed straightforward numerical solutions involving square roots and even transcendental functions of operators. In this section we discuss, though do not prove, the necessity of using the spinless Salpeter equation in place of a Klein-Gordon type equation when dealing with a pure vector potential.

Starting from the simple classical Lagrangian,

$$L = -(m + S(r))\sqrt{1 - v^2} - V(r), \quad (2.1)$$

describing a particle of mass m moving with velocity v in a Lorentz scalar potential $S(r)$ and a Lorentz time-

component vector potential $V(r)$, we find that the Hamiltonian,

$$H = \pm\sqrt{p^2 + (m + S(r))^2} + V(r), \quad (2.2)$$

has a sign ambiguity. This ambiguity arises from the elimination of the velocity in favor of the momentum

$$\mathbf{p} = \frac{\partial L}{\partial \mathbf{v}} = (m + S(r))\gamma \mathbf{v}, \quad (2.3)$$

where $\gamma = (1 - v^2)^{-1/2}$. The positive sign in Eq. (2.2) corresponds to the usual positive energy states and yields the correct non-relativistic limit

$$H \xrightarrow{|p| \ll m} m + \frac{p^2}{2m} + S(r) + V(r). \quad (2.4)$$

The squared form of Eq. (2.2),

$$(H - V(r))^2 = p^2 + (m + S(r))^2, \quad (2.5)$$

known as the generalized Klein-Gordon (GKG) equation, behaves quite differently in the cases of a pure vector and a pure scalar potential. This difference is most easily seen from consideration of the s-wave turning points, where $p^2 = 0$. Eq. (2.2) determines the energy as a function of the potentials at the turning points,

$$E = \pm(m + S) + V. \quad (2.6)$$

We show this turning point condition separately for pure scalar and pure vector linear confining potentials in Figs. 1 and 2. In Fig. 1 we see that for the pure scalar case there is no overlap of the positive and negative branches of Eq. (2.6). In Fig. 2, on the other hand, we see that for any $E > m$ in pure TCV linear confinement there are states on both positive and negative branches. A completely analogous observation [3] has been made earlier in the context of the Dirac equation.

Since the GKG equation (2.5) is quadratic and contains both branches of Eq. (2.2), it can have no normalizable solutions in pure TCV confinement because there is tunneling to the negative energy states, which becomes catastrophic for small quark mass. This difficulty is the well-known ‘‘Klein Paradox’’ [4]. On the other hand, the GKG equation with pure scalar confinement does have well defined normalizable solutions because there is no possibility of tunneling to the negative branch.

The spirit of the Salpeter equation [5] is to conserve a definite particle number. To this end, energy projection operators are employed to remove the negative energy spectrum and the fermion TCV Salpeter equation has normalizable solutions for confined quarks [3]. The spinless Salpeter equation for TCV confinement achieves the same end more simply by explicitly including only the positive branch of Eq. (2.2). For p-wave and higher angular momentum states, we consider the Hamiltonian in spherical coordinates,

$$H = \sqrt{p_r^2 + \frac{J^2}{r^2} + m^2} + ar, \quad (2.7)$$

which we obtain from dividing the momentum into radial and angular parts. The wave equation to be solved is then the eigenvalue problem

$$H|\psi\rangle = E|\psi\rangle \quad (2.8)$$

for the pseudo-differential operator given by Eq. (2.7) with the usual operator replacements.

III. SEMI-CLASSICAL ANALYTIC QUANTIZATION

We have discussed the necessity of using the SS equation instead of the GKG equation with vector confinement. In semi-classical language, the necessity of using the SS equation becomes the necessity of using the turning points given by Eq. (2.6) with the positive sign only. In this section we calculate the semi-classical spectrum of the SS equation with TCV confinement. We first rewrite the SS equation (2.7) in terms of dimensionless variables

$$\begin{aligned} x &\equiv \frac{ar}{E}, \\ \beta &\equiv \frac{aJ}{E^2}, \\ P_r &\equiv \frac{p_r}{E}. \end{aligned} \quad (3.1)$$

In the case of a massless quark, we have

$$\begin{aligned} P_r &= \frac{\sqrt{Q}}{x}, \\ Q &\equiv (x - x_{1-})(x - x_{2-})(x_{1+} - x)(x_{2+} - x), \end{aligned} \quad (3.2)$$

where

$$\begin{aligned} x_{1\pm} &= \frac{1}{2} \left(1 \pm \sqrt{1 - 4\beta} \right), \\ x_{2\pm} &= \frac{1}{2} \left(1 \pm \sqrt{1 + 4\beta} \right). \end{aligned} \quad (3.3)$$

The dimensionless physical turning points resulting from the SS equation are $x_{1\pm}$. The dimensionless constants $x_{2\pm}$ are turning points of the GKG equation, but not of the SS equation.

In the regime we are investigating the angular momentum J is limited but the energy E is large. It follows that $\beta \ll 1$. To see this, we note that even for the leading (circular orbit) Regge trajectory $J/E^2 = 1/4a$ (see the appendix) and hence $\beta_{\text{leading}} = 1/4$. For fixed J and large E , β becomes small. In this limit the leading behavior of the roots (3.3) is

$$\begin{aligned} x_{1-} &= \beta + \beta^2 + \dots, & x_{1+} &= 1 - \beta - \beta^2 - \dots, \\ x_{2-} &= -\beta + \beta^2 + \dots, & x_{2+} &= 1 + \beta - \beta^2 + \dots. \end{aligned} \quad (3.4)$$

The SS equation may be quantized semi-classically by the usual method [6]

$$\int_{r_-}^{r_+} dr p_r = \pi \left(n + \frac{1}{2} \right). \quad (3.5)$$

In dimensionless variables (3.1), the quantization condition (3.5) becomes

$$\int_{x_-}^{x_+} dx P_r(x) = \frac{a\pi}{E^2} \left(n + \frac{1}{2} \right). \quad (3.6)$$

The TCV quantization is achieved by integrating Eq. (3.2). The method is quite accurate for all states and becomes exact for states with many nodes in the radial wavefunction. This is the regime we are particularly interested in.

Although the integral of Eqs. (3.2), (3.6) can be expressed in terms of elliptic integrals, it is more efficient to approximate the integrand first for small β . The approximation

$$\frac{\sqrt{Q}}{x} \simeq \frac{\sqrt{(x - x_{1-})(x - x_{2-})}}{x} \left[1 - x - \frac{\beta^2}{2(1-x)} - \beta^2 \right] \quad (3.7)$$

reproduces the exact integrand to better than 0.5% throughout most of the region of integration, even when $\beta = 0.1$. The accuracy of this approximation is shown graphically in Fig. 3, where we plot both the exact integrand (3.2) and the approximation (3.7) for $\beta = 0.1$.

With the approximation (3.7), the quantization integral (3.6) is relatively easily evaluated. To order β we find

$$\int_{x_-}^{x_+} \frac{\sqrt{Q}}{x} dx \simeq \frac{1}{2} - \frac{\pi\beta}{2} + \mathcal{O}(\beta^2), \quad (3.8)$$

which immediately leads to the result

$$\frac{E^2}{\pi a} = J + 2n + 1. \quad (3.9)$$

Upon making the Langer [7] correction to take into account the centrifugal singularity,

$$J \rightarrow J + \frac{1}{2}, \quad (3.10)$$

where J is now the angular momentum quantum number, we find the final spectroscopic relation

$$\frac{E^2}{\pi a} = J + 2n + \frac{3}{2}. \quad (3.11)$$

The relation (3.11) is identical to an analytic approximation for highly radially excited QCD string, as well as being an excellent approximation to its exact numerical solution [8].

IV. COMPARISON TO EXACT NUMERICAL RESULTS

We can nail down our central result that the QCD string spectrum (3.11) is replicated in the radially dominant regime of the TCV potential by solving the TCV SS equation exactly numerically. The variational (Galerkin) method is well suited for solving eigenvalue equations with mixed coordinate and momentum operators. Briefly, the method begins with a complete set of orthogonal states that can be Fourier transformed. The wavefunction is approximated as a superposition of the lowest N of those states. The wave equation transforms into an $N \times N$ matrix equation which is then diagonalized. The accuracy of the resulting eigenvalues and wavefunctions is measured by the dependence on N and the dependence of the scale parameter of the basis set. Details can be found in [9]. Some further considerations of the accuracy of the variational method are presented in [10].

The TCV SS equation (2.7) with $m = 0$ can thus be solved for a variety of angular momenta, $J = 0, 1, 2, \dots$ and radial states, $n = 0, 1, 2, \dots$. The result is depicted in Fig. 4. Plotted on this figure are both the QCD string slope $1/\pi a$ (solid) and the usual leading trajectory TCV slope $1/4a$ (dashed). In both cases we start the lines at $J = 0$. Although the leading trajectory ($n = 0$) agrees with the dashed prediction, the situation changes as we examine the higher radial excitations. At the larger n values (deep daughters) we observe that the solid line corresponding to the QCD string slope becomes accurate.

In Table 1 we provide the exact and the string solutions for the s-wave radial excitations. We see now that all aspects of the QCD string result (3.11) work quite well. The difference between excitations is accurately two units of $E^2/\pi a$ and the absolute values of the state energies correspond well to the QCD string to three significant figures.

V. SUMMARY AND DISCUSSION

On occasion, some simple results are quite unexpected. We did not expect to find the $m = 0$ QCD string spectroscopy in a potential model. To summarize our finding, we have examined both numerically and analytically the state spectroscopy for a massless quark moving in the

time-component vector linear confinement potential. For states with angular momentum much less than the number of nodes we find the spectrum is exactly that of the QCD string. The Regge slope, radial excitation energy, and the absolute values of the energy (3.11) are exactly what one expects from the QCD string.

Simple results, even surprising ones, usually have simple explanations. As we have recently pointed out [8], the QCD string equations reduce to the spinless Salpeter equation with a linear time-component vector potential for the s-wave states. Thus there is a natural physical connection between the two systems. We can understand this connection simply. A QCD string corresponds to a constant chromoelectric field in the quark rest frame. In the limit that the quark is moving radially, the QCD string has no angular momentum. The total energy of the system becomes

$$E_{\text{string}} = \sqrt{\mathbf{p}^2 + m^2} + ar \frac{\arcsin v_{\perp}}{v_{\perp}} \xrightarrow{v_{\perp} \rightarrow 0} \sqrt{p_r^2 + m^2} + ar. \quad (5.1)$$

In a potential model the field never carries angular momentum. The potential energy of the quark is linear in the distance from the origin, which is the same as the energy of the string as long as the string is moving radially so that there are no relativistic corrections due to its transverse motion. The total energy of the quark in a TCV potential,

$$E_{\text{TCV}} = \sqrt{\mathbf{p}^2 + m^2} + ar, \quad (5.2)$$

in the limit of vanishing v_{\perp} becomes

$$\lim_{v_{\perp} \rightarrow 0} E_{\text{string}} = \lim_{v_{\perp} \rightarrow 0} E_{\text{TCV}} = \sqrt{p_r^2 + m^2} + ar. \quad (5.3)$$

It is thus natural to expect agreement between string and TCV confinement in the radial dominant regime.

The real puzzle is why the Regge slope of the QCD string should be the same for both circular and radial motions. On one hand it is well known from Nambu-Goto days that the Regge slope of a rotating QCD string with one end fixed is $1/\pi a$. We have seen that the TCV potential Regge slope varies from $1/4a$ to $1/\pi a$ as one goes from orbital to radial motion [see Fig. 4]. There is thus no obvious reason why this should not happen with the QCD string. Since the QCD string/TCV potential Regge slopes coincide at $1/\pi a$ for nearly radial motions this explains the remarkable uniform Regge structure seen previously from numerical solutions of the QCD string [8].

Acknowledgments

This work was supported in part by the US Department of Energy under Contract No. DE-FG02-95ER40896.

APPENDIX A: NEARLY CIRCULAR ORBITS

For completeness we semi-classically quantize the TCV equation for nearly circular orbits ($J \gg n$). Using the notation of Eqs. (3.1–3.3), we consider the orbitally dominant regime. In this case the turning points x_{1+} and x_{1-} are nearly equal. By Eq. (3.3), this occurs exactly at

$$\begin{aligned} x_c &= \frac{1}{2}, \\ \beta_c &= \frac{1}{4}. \end{aligned} \quad (\text{A1})$$

For nearly circular orbits we can expand in β and x , giving

$$\begin{aligned} x_{1\pm} &= \frac{1}{2} \pm \sqrt{\frac{1}{4} - \beta} \\ Q &\simeq \frac{1}{16} - \beta^2 - \frac{1}{2} \left(x - \frac{1}{2}\right)^2 \end{aligned} \quad (\text{A2})$$

$$\simeq \frac{1}{2}(x - x_{1-})(x_{1+} - x)$$

Using the quantization condition (3.6), we obtain

$$\frac{1}{2\sqrt{2}} \left(1 - 2\sqrt{\beta}\right) = \frac{a}{E^2} \left(n + \frac{1}{2}\right), \quad (\text{A3})$$

with $\beta = aJ/E^2$. Solving for $\sqrt{\beta}$, squaring and dropping the small squared n/E^2 term, we obtain

$$\frac{E^2}{4a} = J + \sqrt{2}n + \frac{1}{\sqrt{2}}. \quad (\text{A4})$$

Finally, we make the Langer [7] correction $J \rightarrow J + \frac{1}{2}$ and find [8]

$$\frac{E^2}{4a} = J + \sqrt{2}n + \frac{1}{2} + \frac{1}{\sqrt{2}}. \quad (\text{A5})$$

-
- [1] T. J. Allen, M. G. Olsson, and S. Veseli, Phys. Rev. D **62**, 094021 (2000).
 - [2] S. Jacobs, M. G. Olsson, and C. J. Suchyta, Phys. Rev. D **33**, 3338 (1986); Erratum-ibid. D34 3536 (1986).
 - [3] M. G. Olsson, S. Veseli, and Ken Williams, Phys. Rev. D **51**, 5079 (1995).
 - [4] O. Klein, Z. Phys. **53**, 157 (1929).
 - [5] E. Salpeter, Phys. Rev. **87**, 328 (1952).
 - [6] See, for example, L. D. Landau and E. M. Lifshitz, *Quantum Mechanics* (Pergamon, Oxford, 1977)
 - [7] R.E. Langer, Phys. Rev. **51**, 669 (1937); M.S. Child, *Molecular Collision Theory* (Academic, New York, 1974).
 - [8] T. J. Allen, C. Goebel, M. G. Olsson, and S. Veseli, Phys. Rev. D **64**, 094011 (2001).
 - [9] M.G. Olsson, S. Veseli and K. Williams, Phys. Rev. D **51**, 5079 (1995).
 - [10] W. Lucha, F. F. Schöberl, Int. J. Mod. Phys. A **15** 3221 (2000); Phys. Rev. A **60**, 5091 (1999).

TABLE I: An exact numerical solution for s-wave TCV confinement compared with the analytic approximation to the TCV/string showing the rapid convergence of our WKB approximation as the number of radial nodes, n , increases.

n	Exact $\left(\frac{E^2}{\pi a}\right)$	$2n + \frac{3}{2}$
0	1.59	1.50
1	3.53	3.50
2	5.52	5.50
3	7.51	7.50
4	9.51	9.50
5	11.51	11.50
6	13.51	13.50
7	15.51	15.50
8	17.51	17.50
9	19.51	19.50
10	21.51	21.50

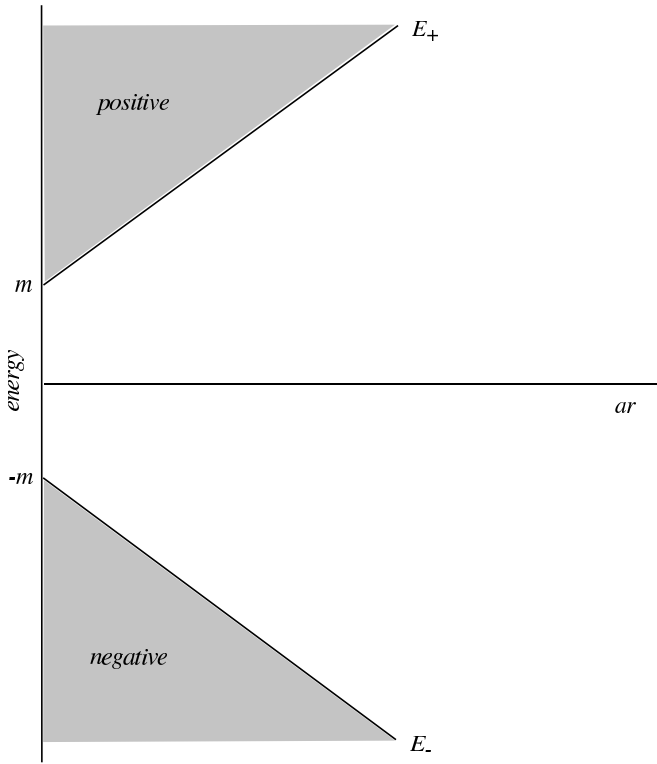


FIG. 1: S-wave classical turning points for Eq. (2.6) with scalar confinement.

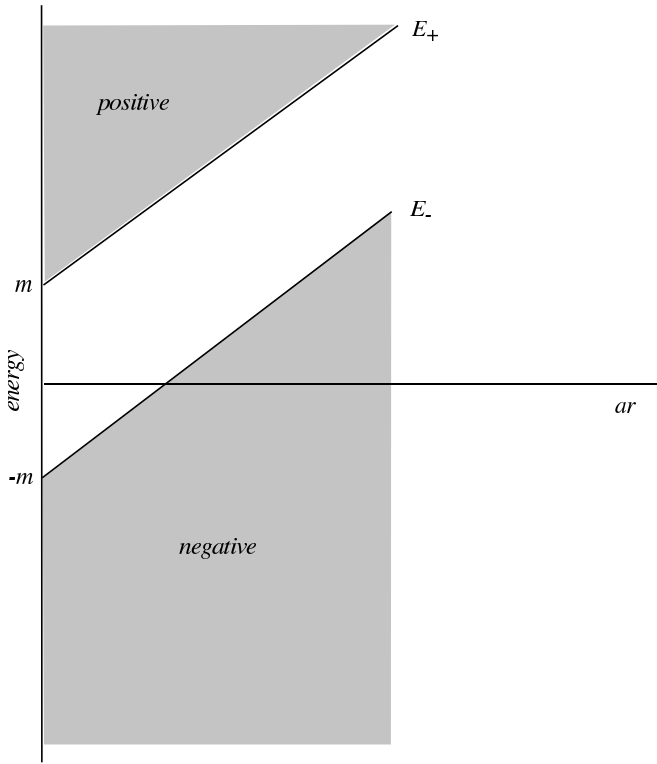


FIG. 2: S-wave classical turning points for Eq. (2.6) with vector confinement.

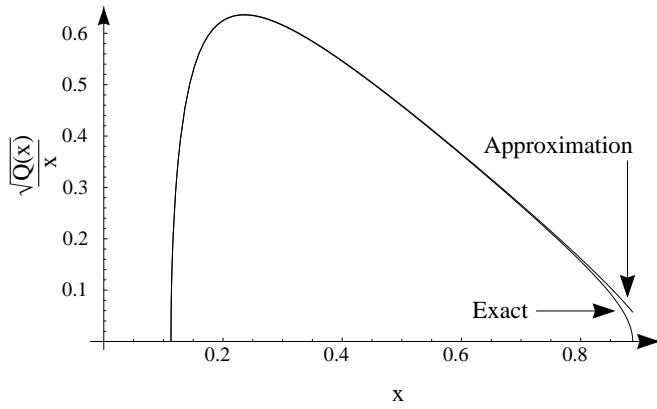


FIG. 3: The exact Bohr-Sommerfeld integrand (3.2) and the approximation (3.7) for $\beta = 0.1$.

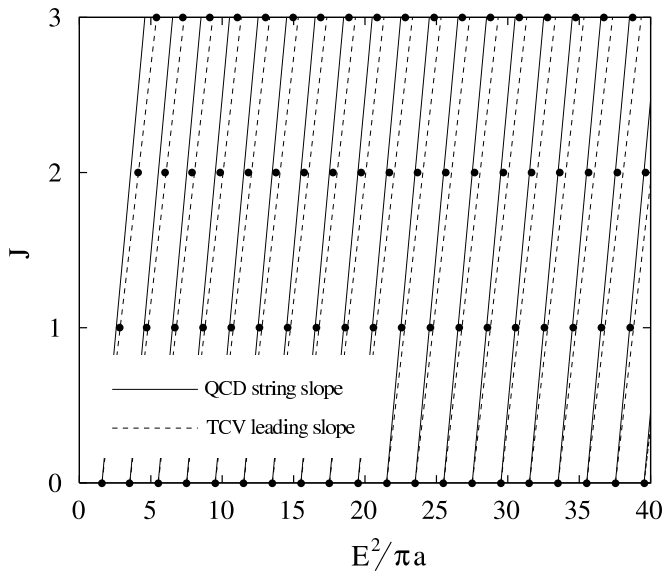


FIG. 4: Regge diagram of exact numerical solutions to Eq. (2.8) with linear vector confinement (dots). The solid lines are the QCD string trajectories with slope $1/\pi a$ and the dashed lines have slope $1/4a$. We observe the transition from the leading TCV slope to string slope.